The xanthophyll cycle affects reversible PsbS-LHCII interactions to control non-photochemical quenching.

Joanna Sacharz, Vasco Giovagnetti, Petra Ungerer, Giulia Mastroianni and Alexander Ruban*

School of Biological and Chemical Sciences, Queen Mary University of London, Mile End Road, London, E1 4NS, United Kingdom

* Corresponding Author: Alexander Ruban (a.ruban@qmul.ac.uk).

Running Title:

The PsbS-LHCII interactions

Keywords: PsbS, LHCII antenna, NPQ, photosystem II, pull-down assay, immunogold labelling

ABSTRACT

To maintain high photosynthetic rates plants must adapt to their light environment on timescale of seconds to minutes. Therefore the light harvesting antenna system of photosystem II (LHCII) in thylakoid membranes has a feedback mechanism, which determines the proportion of absorbed energy dissipated as heat: non-photochemical chlorophyll fluorescence quenching (NPQ). This is crucial to prevent photo-oxidative damage to photosystem II and is controlled by the transmembrane pH differences (ΔpH). High ΔpH activates NPQ by protonation of the protein PsbS and the enzymatic de-epoxidation of LHCII bound violaxanthin to zeaxanthin. But the precise role of PsbS and its interactions with different LHCII complexes remain uncertain. We have investigated PsbS-LHCII interactions in native thylakoid membranes using magnetic bead-linked antibody pull-downs. The interaction of PsbS with the antenna system is affected both by ΔpH and the level of zeaxanthin. In the presence of ΔpH alone PsbS is found mainly associated with the trimeric LHCII protein polypeptides, lhcb1, lhcb2 and lhcb3. However a combinations of ΔpH and zeaxanthin increases the proportion of PsbS bound to the minor LHCII antenna complex proteins lhcb4, 5 and 6. This pattern of interactions was not influenced by the presence of PSII reactions centers. Like LHCII particles in the photosynthetic membrane, PsbS protein forms clusters in the NPQ state. NPQ recovery in the dark required uncoupling of PsbS. We suggest that PsbS acts as a 'seeding' center for the LHCII antenna rearrangement involved in NPQ.

INTRODUCTION

In order to cope with rapid fluctuations in light intensity, plants have evolved optimized multilevel mechanisms that enable the capture of sufficient light energy under limiting conditions, while efficiently dissipating excess light energy. One of the most significant mechanisms ensuring protection of plants from high light intensities is non-photochemical chlorophyll fluorescence quenching (NPQ)[1]. In plants, photosystem II (PSII) receives absorbed light energy from the peripheral antenna system, which consists of nuclear-encoded pigment binding protein

complexes[2]. PSII light-harvesting complexes (LHCIIs) include the major LHCII trimers (comprising of lhcb1, lhcb2 and lhcb3 polypeptides) and minor LHCII monomers: CP29 (lhcb4), CP26 (lhcb5) and CP24 (lhcb6) complexes[2]. Chlorophylls and carotenoids bound to LHCs absorb light energy and then transfer it to the PSII reaction centers (RCII), where charge separation occurs. However, in high light conditions the amount of light absorbed by the antenna exceeds that which can be used by RCII in photosynthesis. This excess absorbed energy can cause photo-oxidative damage to RCII, a condition known as photoinhibition[3-7], which significantly decreases photosynthetic productivity. NPQ is the most rapid and efficient mechanism of dissipation of excess absorbed light energy into heat[8-11]. It is a complex process and a complete understanding of its mechanism has not yet been achieved. In recent years, several crucial factors were found to trigger NPQ formation. The primary and fastest NPQ component, called qE (energy-dependent quenching), depends on the generation of a pH gradient across the thylakoid membranes[8,9,11]. The acidification of the thylakoid lumen is essential for NPQ induction[8,12], most probably by facilitating protonation of certain aspartate and glutamate residues within LHCII complexes[8,10,13], as well as the conversion of violaxanthin into zeaxanthin[14,15]. In addition, a third essential component, the PsbS protein, was discovered by Niyogi and co-workers and shown to respond to proton gradient changes[16,17]. The recently published PsbS crystal structure suggests that this four transmembrane helix member of the light-harvesting complex (LHC) superfamily is a non-pigment binding protein, taking it off the list of potential candidates for a direct NPQ quencher[18]. Furthermore, the authors of this report found PsbS as homodimer both in light-harvesting and NPQ states of the antenna[18]. However, these data are based on *in vitro* experiments where pH was artificially decreased and they are not consistent with previous *in vivo* studies of PsbS dynamics, showing that the dimeric protein becomes a monomer upon NPQ formation[19-22]. Furthermore, the exact mechanics of NPQ catalysis by PsbS remains unknown. Indeed, it is still a matter of debate whether PsbS is associated with PSII core[22] or not[23,24], whilst other groups suggest that only PsbS monomers are found within the major trimeric LHCII domain[19].

The NPQ mechanism also involves the conversion of violaxanthin into zeaxanthin. *In vitro* studies showed that the incorporation of both PsbS and zeaxanthin promoted LHCII aggregation in proteoliposomes, but neither zeaxanthin nor PsbS alone were effective in inducing the quenching[21]. The role of zeaxanthin and the mechanism of its action in NPQ formation is controversial. Comprehensive studies on fluorescence quenching revealed that plants with light-

induced zeaxanthin establish larger NPQ and it appears that zeaxanthin formation shapes the photosynthetic membrane into a responsive state against high light exposure, by enhancing the rate of NPQ formation and slowing down the relaxation rate[11]. Differently, the presence of PsbS promotes a quick and enhanced NPQ development, as well as improving NPQ recovery in the dark, as shown by experiments performed on the PsbS-overexpressing mutant (*L17*)[25,26]. It is agreed that PsbS and zeaxanthin have a synergistic effect on photoprotection[11].

The complexity of the NPQ mechanism could rely upon tuning LHCII antenna sensitivity to lumen pH[11]. Such a fine functional adjustment would involve zeaxanthin, LHCII aggregation and PsbS protein working together in order to increase the pKa for protonation of LHCII complexes[11]. We designed this study to find out which complexes PsbS interacts with in the grana membrane, how these interactions are affected by NPQ and zeaxanthin, and whether PsbS converts its molecular structure during the NPQ state.

RESULTS

PsbS binding to LHCII antenna complexes

We optimized a magnetic bead-linked antibody pull-down assay to map PsbS interactions. The main advantage of this technique over other standard procedures is that it allowed us to work with small-scale thylakoid membrane preparations and limit the number of preparative prolonged steps during the pull-down procedure, potentially affecting protein interactions. Additionally, we carefully chose an appropriate cross-linker, dithiobis[succinimidyl propionate] (DSP), which is hydrophobic and easily diffuses through the chloroplast membrane. Furthermore, DSP shows a short cleavable arm binding amine groups of 12 Å and quickly works at low concentration.

Inspection of thylakoid membrane proteins separated by denaturing SDS-PAGE revealed that our pull-down assays preserved interactions of PsbS with various LHCII antenna complexes in the oligomeric structure visible at around 115 kDa (Fig. 1a and 2a) (for details see *Materials and Methods*). This complex was mostly present in the NPQ state and enhanced upon cross-linking. In chloroplasts containing only violaxanthin, PsbS appeared to mainly interact, in most of the tested conditions, with lhcb1 subunit of LHCII complex and minor antenna polypeptides (most strongly with CP29) (Fig. 1b). In the dark, PsbS was associated with LHCII trimers and CP29. In the NPQ

state, we observed a significant increase in interactions with lhcb1, and to a less extent with lhcb2 and lhcb3. A small increase in PsbS interaction with CP29 was also observed during the transition from dark to NPQ state, together with PsbS interactions with the polypeptides of CP26 and CP24 complexes (Fig. 1b). Interestingly, during relaxation there was a significant loss of PsbS affinity to lhcb1, while it bound to CP24 and CP26 minor antenna complexes more strongly. DSP addition did not alter significantly the pattern of PsbS binding, however lhcb1 polypeptide seemed to be a preferential target for protein interaction in the dark and NPQ state, in contrast to recovery state (Fig. 1b). CP29 revealed again a strong affinity to PsbS in the NPQ state, which was reversible during dark relaxation, unlike the binding to CP24 and CP26 (Fig. 1b).

Taking into consideration that NPQ involves PSII antenna reorganization[11] and the use of a cross-linker may have affected this process, we tested how different concentrations of DSP influenced NPQ formation and relaxation, and whether it had an impact on PsbS binding. Only when a low DSP concentration (0.5-1.0 mM) was employed, the NPQ formation rate was not significantly disturbed in comparison to control (Supplementary Fig. 1a). However, the cross-linker strongly inhibited relaxation in all tested concentrations. This effect was accompanied by the formation of an oligomeric band at ~115 kDa that contained the PsbS protein (Supplementary Fig. 1b). These data suggest that NPQ recovery in the dark required PsbS mobility in the thylakoid membrane in order to uncouple from the observed oligomeric complex of interacting antenna subunits.

Impact of xanthophyll cycle activation on PsbS binding to LHCII antenna complexes

PsbS interactions were also assessed in chloroplasts enriched with zeaxanthin. In agreement with previous results[1], chloroplasts isolated from zeaxanthin-enriched leaves showed faster and greater NPQ induction, as well as a lower rate of recovery in comparison to the values measured on violaxanthin-enriched chloroplasts (compare Fig. 1c and 2c). PsbS interactions in zeaxanthin-enriched membranes were also altered. Dark-adapted zeaxanthin-containing chloroplasts showed a significantly reduced interaction with lhcb1 but increased affinity to lhcb2, lhcb3 and minor antenna complexes (Fig. 2b). Oligomeric forms of PsbS-lhcb polypeptides were present even under denaturing and reducing conditions mainly in the NPQ state (Fig. 2a). Upon illumination PsbS was found interacting with the minor antenna CP24, CP26 and CP29 complexes. After NPQ recovery, PsbS clearly released from these complexes, in contrast to membranes containing only violaxanthin (compare Fig. 1b with Fig. 2b). These results may be explained by more drastic

structural changes in PSII antenna organization after zeaxanthin synthesis. The use of DSP largely promoted all interactions during both NPQ and recovery states. While NPQ recovery significantly promoted PsbS-lhcb1 interactions, it caused decreased binding between PsbS and lhcb3 (Fig. 2b). PsbS release from CP29 complex during NPQ relaxation was instead consistent in both, violaxanthin and zeaxanthin containing membranes (Fig. 1b and Fig. 2b).

Effect of the presence of photosystem II reaction centers on PsbS binding patterns

Previous studies suggested that PsbS is associated with RCII[22]. Our western blots, however, reveal no presence of D1 protein in pull-down eluted samples (Fig. 1d). To further investigate how the presence of RCII impacts PsbS binding patterns, we used PsbS overexpressing *A. thaliana L17* plants treated with lincomycin, which are deprived of RCII[27,28], hence enhancing the amount of PsbS-bound material and NPQ levels. Two weeks of antibiotic treatment resulted in the inhibition of chloroplast-encoded proteins causing a significant decrease in the content of RCII, as well as CP43 and CP47 inner antenna complexes. Loss of the entire core complex structure was previously achieved in more than 80% of PSII units in *A. thaliana*[27,28]. This was accompanied by a strong decrease in PSII quantum efficiency (Fv/Fm) to 0.2, and the capacity to form larger NPQ than that measured in untreated chloroplasts (Supplementary Fig. 2). The amount of antenna proteins was normalized relative to the total amount of PsbS in the elution. Overall, *L17* mutant chloroplasts showed a greater amount of PsbS in the thylakoid membranes and higher abundance of PsbS in the pull-down assays in comparison to control plants (Supplementary Fig. 2). In chloroplasts with greatly reduced amounts of RCII, PsbS largely bound to CP29 even in the membranes containing violaxanthin (Supplementary Fig. 2). A greater exposure of CP29 to PsbS in thylakoid membranes depleted of RCII might explain such results. Furthermore, this is also consistent with previous findings showing that violaxanthin de-epoxidation promotes CP29 energetic coupling to the bulk of LHCII, while reducing its connectivity to PSII core antenna[29]. Overall, these functional alterations increase the probability for PsbS-CP29 interactions. We believe that a comparable scenario is likely to take place in lincomycin-grown plants where CP29 is much looser relative to untreated plants. Moreover, the addition of DSP significantly enhanced the pull-down elutions of CP24 and CP26 proteins, highlighting its effect on PsbS binding to the minor antenna once PsbS is overexpressed and minor antenna complexes are free from RCII interactions.

The presence of PsbS in the NPQ state within LHCII oligomers

In order to further probe whether PsbS is associated with light-induced aggregated LHCII we prepared native thylakoid membranes from *A. thaliana L17* plants, by lightly solubilizing with low concentrations of mild detergents. Samples were then subjected to separation on a size exclusion chromatography column. Parallel zeaxanthin-enrichment and NPQ formation caused an increase in the amount of heavy fractions eluted between 18 and 20 min. These fractions contained mainly aggregated LHCII antenna complexes that included Lhcb1 and CP29 polypeptides (Fig. 3). In addition, whilst PsbS protein in the dark was detectable mostly in the lighter fractions eluted between 26 and 30 min, in zeaxanthin-containing membranes in NPQ state PsbS appeared as a strong component of the heavy LHCII oligomer fractions (B9 and B10). Similar results were observed for CP29, whose abundance increased over 5 times in the fractions B9 and B10 where PsbS was also present.

Clustering of PsbS in the NPQ state

Immunogold labelling electron microscopy was used to address and visualize PsbS localization and dynamics during the NPQ state in the thylakoid membrane. PsbS antibody was employed as primary, followed by a secondary antibody coupled with 10 nm colloidal gold. *A. thaliana npq4* mutant (PsbS knockout) and spinach chloroplasts without application of primary antibody during immunogold labelling served as control samples and showed no gold particles, indicating the PsbS-antibody specificity of the adopted labelling procedure (Supplementary Fig. 3). Fig. 4a displays thin section images revealing PsbS binding patterns in dark-adapted and zeaxanthin-containing illuminated thylakoid membranes. Despite the high number of gold labeled PsbS in both conditions, the gold particles in dark-adapted chloroplasts were more sparsely distributed, while PsbS was visibly accumulating in small areas in those illuminated (Fig. 4a and b). NPQ induction in zeaxanthin-enriched chloroplasts resulted in over 60% increase of the overall particle number (Fig. 4c). This is in agreement with the occurrence of light-induced change in the quaternary structure of PsbS from dimers populating the antenna light harvesting state (in the dark) to monomers upon NPQ formation, as previously proposed[19,20]. The coordinates of particles picked from both dark-adapted and illuminated samples (more than 30000 particles from biological triplicates) were used to calculate the number of particles within a 50 nm radius area. A significant increase in the number of PsbS protein clusters was found in relation to NPQ induction (Fig. 4b). More than 55% of PsbS proteins resulted in clusters of 5 particles on average within a

50 nm radius area. In contrast, in dark-adapted samples, the same percentage had on average only 1-2 neighboring particles within the same area. These data support the fact that the changes in PsbS reorganization in the NPQ state mirror LHCII rearrangement, as observed by freeze-fracture electron microscopy earlier[30].

DISCUSSION

Here we show a novel approach to study membrane protein interactions in transient states employing efficient and relatively fast pull-down assays coupled with the addition of a hydrophobic cross-linker. Using this method, we determined PsbS interactions established with PSII antenna complexes during NPQ kinetics of induction and recovery. Overall, our data support recent reports[22,23] showing that PsbS interactions with LHCII trimers take place in the dark and are further enhanced in the NPQ state[23]. However, we found that PsbS interacts not only with LHCII trimers, specifically M trimer (lhcb1, Fig. 5), as proposed by Gerotto and co-authors[22], but also with the minor antenna complexes, CP24, CP26 and CP29 (Fig. 1, 2 and 5). Gerotto and co-workers only found trace amounts of PsbS interacting with the PSII core[23]. Our results also revealed minor to none PsbS interactions with RCII, in contrast to the data reported by Correa-Galvis and co-workers[23]. Several methodological considerations and differences between the procedures adopted in our study and in the work of Correa-Galvis et al.[23] can explain such discrepancy. Firstly, it is reasonable to think that the fact that we used 5-times lower concentrations of a hydrophobic cross-linker (DSP) minimized the number of cross-linked proteins, relative to Correa-Galvis et al.[23], who instead added a hydrophilic cross-linker and at higher concentration. Secondly, our pull-down assays on small-scale material were accomplished within 2.5 hours, thus limiting the probability of protein aggregation and artificial interactions. Additionally, despite denaturing and reducing conditions in SDS–PAGE were applied, the oligomeric complexes of PsbS-lhcb (~115 kDa) prevailed in our experiments even prior to the use of DSP (Fig. 1a and 2a). These higher molecular weight complexes were detected mainly in the NPQ state and were less abundant during NPQ recovery, suggesting that the affinity of PsbS towards lhcb proteins is higher upon illumination and NPQ formation. The existence of high molecular weight oligomers of PsbS and lhcb polypeptides in a denaturing gel may be due to the capacity of our pull-down method to effectively preserve strong hydrophobic interactions between membrane proteins. Indeed,

protonation of the highly hydrophobic PsbS and lhcb proteins can establish unusually strong associations between them, which resist even gel denaturation.

In our study, we also assessed protein binding/interaction experiments on chloroplasts in NPQ state and enriched in zeaxanthin, as well as on chloroplasts dark-exposed to relax the quenching, hence tackling the short-term reversibility of PsbS binding dynamics. Zeaxanthin enhanced PsbS binding to the minor antenna complexes even in the dark, most significantly to CP29 polypeptides (Fig. 2). This binding was further increased in the NPQ state and, most importantly, was highly reversible after NPQ recovery. Unlike chloroplasts containing only violaxanthin (Fig. 1), the reversibility of PsbS binding was also significant for CP24 and CP26 polypeptides (Fig. 2). The formation of zeaxanthin appeared thus to have caused some LHCII antenna reorganization, which makes PsbS become more accessible to the minor antenna complexes CP24 and CP26, even in the dark. This is consistent with results presented in our previous work that used excitation fluorescence spectroscopy to detect alterations in energy relations between PSII core, LHCII trimers and aggregates, as well as CP29 complex[30]. It was proposed that zeaxanthin promoted interaction of CP29 with the bulk of oligomeric LHCII[30]. Here, using gel filtration of gently solubilized thylakoid membranes from lincomycin-treated *A. thaliana L17* plants, we confirm this proposal biochemically (Fig. 3). Our results indeed show that the presence of zeaxanthin during NPQ promotes the formation of large LHCII oligomers that contain not only PsbS but are enriched in CP29 complexes. This scenario is further supported by the evidence that PsbS and LHCII clustering is enhanced when the antenna adopts a dissipative state (Fig. 4 and 5). PsbS may therefore act as an aggregation promoter rather than a substrate binding to RCII, thus favoring LHCII dissociation and rearrangement towards the optimization of the photoprotective state. Indeed, recent work performed on the membranes of lincomycin-treated plants containing different levels of PsbS has provided a spectroscopic evidence for the LHCII antenna aggregation-promoting effect of PsbS, which correlated with the extent of NPQ[31].

PsbS interactions with LHCII proteins observed in this study are illustrated in the model presented in Fig. 5. The multiple interaction sites and binding preferences to the minor antenna in the presence of zeaxanthin suggests that PsbS crucially prompts the whole LHCII antenna reorganization. Indeed, it was demonstrated that mutant plants overexpressing PsbS are capable to form enhanced NPQ, as well as more quickly and efficiently recover from it, suggesting that PsbS

plays the role of 'membrane mobilizer'[1,32,33]. Goral and co-workers reported a considerable inhibition in LHCII mobility in the *npq4* mutant lacking PsbS[34], reflecting the need for rapid and effective protein mobility to restore antenna light harvesting. In relation to this aspect, it should be noted that cross-linking inhibited NPQ recovery (Supplementary Fig. 1). The cross-linker might have indeed fixed PsbS in the dimeric structure, preventing its monomerisation. It is therefore likely that PsbS monomers are able to interact more efficiently with the antenna complexes, for instance by exposing their hydrophobic surfaces. However, it is also possible that PsbS dimers cannot effectively bind to LHCII and in particular to more hydrophobic minor antenna complexes during NPQ state.

In conclusion, we found that the dynamics of PsbS binding during zeaxanthin accumulation and NPQ formation is independent of the presence of RCII. In the dark, PsbS is dimeric and localized mainly around the M trimer (Fig. 5). Light induces PsbS monomerisation that promotes its interactions with LHCII antenna, and with particular affinity to CP29 complex. Interactions with CP24 and CP26 are promoted by zeaxanthin even in the dark. PsbS occurs in clusters in the thylakoid membranes during the NPQ state, similarly to the NPQ-induced LHCII aggregation pattern. Given PsbS mobility within the thylakoid membranes, binding to LHCII oligomers along with the CP29 complex, we propose that this protein may play the essential role of LHCII antenna aggregation-enhancer.

MATERIALS AND METHODS

Plant material and treatments. Leaves of spinach (*Spinacea oleracea*, from a local market) and *Arabidopsis thaliana* Columbia (Col-0) ecotype (WT), *L17* (PsbS-overexpressing mutant) and *npq4* (PsbS-deficient mutant) were used in this study. *A. thaliana* plants were grown under 180 µmol photons m^{-2} sec^{-1} in a 12h/12h day/night photoperiod at a temperature of 20 °C. Lincomycin-treatment (0.4 mg/L) was performed on 5 weeks old plants and lasted for 2 weeks or until Fv/Fm was 0.2. Plants subjected to experiments were 7 weeks old. Spinach leaves were enriched in zeaxanthin content by pre-illumination at 300 µmol photons m^{-2} sec^{-1} under 98% N_2/2% O_2 for 1 hour, to inhibit the epoxidation of zeaxanthin into violaxanthin (de-epoxidation state ~ 60%). For

A. thaliana, zeaxanthin was induced illuminating whole plants at 300 µmol photons m^{-2} sec^{-1} for 1 hour. Leaves were collected and dark-adapted in ice-cold water.

Pigment analysis. The total pigment content was estimated according to the method of Porra et al.[35]. Pigments were extracted in 80% ice-cold acetone, followed by 5 min centrifugation at 14000 rpm. Absorbance values at 646.6, 663.6, and 750 nm were detected to determine the chlorophyll concentration. Xanthophyll concentrations were determined by reverse-phase HPLC, using a LiChrospher 100 RP-18 column and Dionex Summit chromatography system[36]. The de-epoxidation state (DES) was determined as DES=(Zea+0.5Ant)/(Vio+Ant+Zea), where Zea, Ant and Vio are the concentration of zeaxanthin, antheraxanthin and violaxanthin, respectively.

PAM fluorescence measurements. Chlorophyll fluorescence induction was measured with a Dual-PAM-100 fluorometer (Waltz). Chloroplasts were resuspended in 1.5 mL of resuspension buffer (0.3 M Sorbitol, 2.5 mM EDTA, 5 mM $MgCl_2$, 10mM $NaHCO_3$, 20 mM HEPES, 0.5% (w/v) BSA, pH 7.6) with a chlorophyll concentration of 35 µg/mL. The fluorescence level with PSII reaction centers open (Fo) was measured with 2 µmol photons m^{-2} s^{-1} measuring beam. The maximum fluorescence values in the dark-adapted state (Fm) and during the course of actinic illumination (Fm') were determined using a 0.8 s saturating light pulse (3000 µmol photons m^{-2} s^{-1}). Fluorescence quenching was induced by 10 min illumination with an actinic light intensity of 450 µmol photons m^{-2} s^{-1} (Fig. 1c and 2c). Such light intensity ensured that the photoinhibition component of NPQ was absent[10,11]. Far red light was used in the dark to enhance Q_A oxidation, during fluorescence recovery. Samples were collected in the dark, NPQ and recovery state for further analysis. DSP (final concentration 0.5 mM) was added to the samples prior to illumination (dark-adapted chloroplasts), after 10 min of illumination (NPQ state) and after 10 min in the dark (NPQ recovery). DSP largely inhibited NPQ recovery. NPQ state was instead sustained by cooling the sample or lowering the incubation buffer pH (5.5).

Isolation of chloroplasts and thylakoid membranes. Chloroplasts were obtained from spinach or 7 week old *A. thaliana* leaves by mechanical disruption in grinding buffer (0.4 M Sorbitol, 2.5 mM EDTA, 5 mM EGTA, 5 mM $MgCl_2$, 10 mM $NaHCO_3$, 20 mM Tricine, 0.5% (w/v) BSA, pH 8.4). Samples were filtered through four layers of muslin cloth, and then four layers of muslin cloth with a layer of non-adhesive cotton, and finally resuspended in resuspension buffer (0.3 M Sorbitol, 2.5 mM EDTA, 5 mM $MgCl_2$, 10 mM $NaHCO_3$, 20 mM HEPES, 0.5% (w/v) BSA, pH

7.6). Thylakoid membranes were prepared by further centrifugation (5 min, 3500 × g, 4 °C) and resuspension in 2 mL of hypotonic buffer (2.5 mM EDTA, 5 mM $MgCl_2$, 10 mM $NaHCO_3$, 20 mM HEPES, 0.5% (w/v) BSA, pH 7.6). Membranes were collected by further 10 min centrifugation at 3500 × g 4 °C and resuspended in 1 mL of resuspension buffer.

Titration of cross-linker and pull-down assay. Working conditions for the cross-linker dithiobis (succinimidyl propionate) (DSP) were optimized by titration of its concentration and incubation time with intact chloroplasts. Based on the analysis of proteins pulled down from dark-adapted and NPQ-induced samples, DSP concentrations (0-1.0 mM) and incubation times (15-30 min) were carefully selected to prevent the occurrence of false positives, altered protein interactions and antenna oligomerization related to PsbS presence, during NPQ formation. Pull-down assays were prepared by first coupling PsbS antibody (Agrisera) to magnetic beads (µMACS, Flexi Kit) according to manufacturer's instructions. 50 µL of α-PsbS-beads were added to 100 µL of thylakoid membranes (100 µg/mL chlorophyll) solubilized in 0.5% β-DM and incubated for 1 hour on ice slightly shaking. The mixture was then loaded in equal volumes and concentrations onto equilibrated columns packed with iron resin (µMACS). Eluted samples were collected promptly followed by 6 washing fractions (Washing Buffer 1 : 150 mM NaCl, 0.5% Igepal CA-630 (v/v), 0.5% sodium deoxycholate (v/v), 0.1% SDS (w/v), 50 mM Tris HCl pH 8.0; Washing Buffer 2: 20 mM Tris HCl pH 7.5). Fractions were eluted by applying 20 µL and 50 µL of elution buffer (at 90 °C (50 mM Tris HCl, pH 6.8), 50 mM DTT, 1% SDS (w/v), 1 mM EDTA, 0.005% bromophenol blue, 10% glycerol (v/v)).

Control PsbS pull-down assays performed on *A. thaliana npq4* mutant (PsbS-deficient) showed no lhcb1 or lhcb4 proteins (i.e. the major interactions observed in this study) binding to the magnetic beads and the resin (Supplementary Fig. 4). To additionally confirm the validity of our method, we coupled PsbS to magnetic beads and visualized the material in the pull-down elution together with interacting immunogold-labelled CP29 protein (Supplementary Fig. 5). The number of antibodies attached to each magnetic bead cannot be accurately determined however there were on average two immunogold-labeled CP29 proteins per 50 nm magnetic bead. The material appeared to be embedded into native membrane, which is expected as PsbS is a four transmembrane protein deeply buried in the membrane. There was an increase in CP29 associated

with PsbS-coated magnetic beads when DSP was used and the number of interactions increased on average to 4 gold particles, in agreement with western blots data.

SDS-PAGE and western blotting. Proteins were resolved by SDS-PAGE. Equal volumes of pull-down fractions or 5 µg chlorophyll of solubilized thylakoid membranes were loaded on 12% acrylamide denaturating gels running constantly at 120 V for 90 min[37]. Gels were either stained by Instant Blue (Expedeon) or used for electroblotting onto nitrocellulose membrane (GE Healthcare). Membranes were probed over night with antibodies (dilution according to manufacturer, Agrisera) and the following day thoroughly washed and incubated with secondary anti-rabbit antibodies (1:20,000, IRDye 800CW, LI-COR).

All nitrocellulose membrane used in this study were scanned and visualized using near-infrared fluorescence detection (Odyssey Imaging System, LI-COR). Generated 16-bit images were exported as tiff files. Freely available ImageJ program was used for quantitative western blot analysis based on comparison of bands densities. Images used for analysis were converted to 8-bit gray-scale. The intensity of each probed protein in each condition was estimated by automatically picking all bands present in each western blot lane. Background signal was subtracted by selecting only the area of each peak above the baseline of profile plot. The values were then summed and further normalized to the total amount of PsbS pull downed in each condition and later averaged for three replicates (Figures 1b and 2b graphic representation = ($lhcb_a/PsbS_a$ + $lhcb_a/PsbS_a$ + $lhcb_a/PsbS_a$)/3).

FPLC. Thylakoid membranes were resuspended in 0.5 mL of breaking buffer (5 mM NaCl, 5 mM $MgCl_2$, 10 mM HEPES, pH 7.5) to a final chlorophyll concentration of 0.5 µg/mL and solubilized on ice for 30 min with 0.2% α-DM (v/v) and 0.5% digitonin (v/v). Samples were briefly spun at 9000 rpm (4 °C) and the supernatant was filtered through filter with 0.44 µm cut off as previously described[36]. 500 µL of each sample were loaded on the S300 22/300 size exclusion column (AKTA system). Fractions were eluted with filtered FPLC buffer (20 mM Bis-Tris, 0.03% α-DM, 5 mM $MgCl_2$) and subjected to further analysis.

Thin-section electron microscopy. Dense pellets of chloroplasts were resuspended in phosphate buffered with 3% paraformaldehyde (w/v) and incubated at room temperature for 15 min. Pellets were washed 3 times with PBS (pH 7.3), resuspended in equal volume of 2% agarose (w/v) at 80

°C and allowed to cool down at RT. Chloroplast-containing solid agar was cut into 1-2 mm cubes and dehydrated by exposure to increasingly concentrated ethanol solutions (30, 50, 70, 90 and 100% (v/v), with each step incubation time of 15 min). Agar cubes were placed in 50% (v/v) ethanol LR White resin for 1 hour at room temperature on a rotator. Samples were moved to fresh LR White resin and incubated for an additional 1 hour. The LR White resin was finally changed and samples were left at room temperature for 48 hours. The final embedding in LR White resin was completed by incubation at 55 °C for additional 48 hours. Thin sections were prepared by cutting solid agar with an ultramicrotome (Reichert-Jung Ultracut E) using a diamond knife and collected onto nickel grids, before further analysis at the transmission electron microscope (Jeol JEM 1230).

Immunogold labeling. Immunogold labeling was performed on thin-sectioned chloroplasts dark-adapted or in NPQ state. Thin-sectioned chloroplasts on nickel grids coated with formvar were washed and blocked by incubation on a drop of PSBS and 5% (w/v) BSA. Samples were subsequently incubated with the primary antibody (anti-PsbS, Agrisera; 1:100), washed in PBS solution and re-probed with secondary anti-rabbit 10 nm colloidal gold antibody (Sigma-Aldrich, 1:100). Grids where then poststained with uranyl acetate and lead citrate and inspected using transmission electron microscopy (TEM). Immunogold labeling for pull-down material required a different protocol designed for exosomes. 5 µL of pull-down suspension (without DTT and detergent) was deposited onto formvar-carbon coated grids. The washing was carried out by transferring the grid upside down inside droplets of the following solutions: 2x PBS, 4x PBS and 50 mM Glycine, 1x PBS and 5% (w/v) BSA (Sigma-Aldrich). Incubation with primary antibody (anti-CP29, Agrisera; 1:100) for 30 min followed by 3 washes in PBS. Incubation with secondary anti-rabbit 10 nm colloidal gold antibody (Sigma-Aldrich, 1:100) for 30 min followed by 8 washes in PBS. Grids were transferred to 1% glutaraldehyde for 5 min and washed 8 times in ddH_2O, prior to TEM analysis. Particle counting in immunogold labeled samples was performed in ImageJ. Particle x and y coordinates of more than 30,000 particles were picked and used for analysis.

DATA AVAILABILITY

The data that support the findings of this study are available from the corresponding author upon request.

REFERENCES

1. Demmig-Adams, B., Garab, G., Adams, III W., Govindjee. Non-photochemical quenching and energy dissipation in plants, algae and cyanobacteria. Advances in photosynthesis and respiration 40. Springer (2014).
2. Jansson, S. A guide to the Lhc genes and their relatives in *Arabidopsis*. *Trends Plant Sci*. **4**, 236–240 (1999).
3. Powles, S.B. Photoinhibition of photosynthesis induced by visible-light. *Ann. Rev. Plant Physiol. Plant Mol. Biol.* **35**, 15–44 (1984).
4. Barber, J. Molecular-basis of the vulnerability of photosystem-II to damage by light. *Aust. J. Plant Physiol.* **22**, 201–208 (1995).
5. Osmond, C.B. What is photoinhibition? Some insights from comparisons of shade and sun plants. Photoinhibition of photosynthesis (eds. N.R. Baker and J.R. Bowyer), pp. 1–24. Lancaster: Bios Scientific Publishers (1994).
6. Demmig-Adams, B. & Adams, W.W. Photoprotection and other responses of plants to high light stress. *Annu. Rev. Plant Physiol. Plant Mol. Biol*. **43**, 599–626 (1992).
7. Li, Z., Wakao, S., Fischer, B.B. & Niyogi, K.K. Sensing and responding to excess light. *Annu. Rev. Plant Biol.* **60**, 239–260 (2009).
8. Horton, P., Ruban, A.V. & Walters, R.G. Regulation of light harvesting in green plants. *Annu. Rev. Plant Physiol. Plant Mol. Biol*. **47**, 655–684 (1996).
9. Niyogi, K.K. & Truong, T.B. Evolution of flexible non-photochemical quenching mechanisms that regulate light harvesting in oxygenic photosynthesis. *Curr. Opin. Plant Biol.* **16**, 307–314 (2013).
10. Ruban, A.V. Evolution under the sun: optimizing light harvesting in photosynthesis. *J. Exp. Bot.* **66**, 7–23 (2015).
11. Ruban, A.V. Non-photochemical chlorophyll fluorescence quenching: mechanism and effectiveness in protection against photodamage. *Plant Physiol.* **170**, 1903–1916 (2016).
12. Kramer, D.M., Sacksteder, C.A. & Cruz, J.A. How acidic is the lumen? *Photosynth. Res*. **60**, 151–163 (1999).
13. Liu, Z. *et al.* Crystal structure of spinach major light-harvesting complex at 2.72 Å resolution. *Nature* **428,** 287–29 (2004).

14. Demmig-Adams, B. Carotenoids and photoprotection: a role for the xanthophyll zeaxanthin. *Biochim Biophys Acta* **1020**, 1–2 (1990).
15. Yamamoto, H. Y., Nakayama, T. O. M. & Chichester, C. O. Studies on the light and dark interconversions of leaf xanthophylls. *Arch. Biochem. Biophys*. **97**, 168–173 (1962).
16. Li, X.P. *et al.* A pigment-binding protein essential for regulation of photosynthetic light harvesting, *Nature* **403**, 391–395 (2000).
17. Li, X.P. *et al.* Regulation of photosynthetic light harvesting involves intrathylakoid lumen pH sensing by the PsbS protein. *J. Biol. Chem.* **279**, 22866–2287 (2004).
18. Fan, M. *et al.*, Crystal structures of the PsbS protein essential for photoprotection. *Nature Struc. Mol. Biol.* **22**, 729–735 (2015).
19. Bergantino, E. *et al.* Light- and pH-dependent structural changes in the PsbS protein of photosystem II. *Proc. Natl. Acad. Sci. U. S. A.* **100**, 15265–15270 (2003).
20. Teardo, E. *et al.* Evidences for interaction of PsbS with photosynthetic complexes in maize thylakoids. *Biochim. Biophys. Acta* **1767**, 703–711 (2007).
21. Wilk, L., Grunwald, M., Liao, P.N., Walla, P.J. & Kühlbrandt, W. Direct interaction of the major light-harvesting complex II and PsbS in nonphotochemical quenching. *Proc. Natl. Acad. Sci. U. S. A.* **110**, 5452–5456 (2013).
22. Gerotto, C., Franchin, C., Arrigoni, G. & Morosinotto, T. *In vivo* identification of photosystem II light harvesting complexes interacting with photosystem II subunit S. *Plant Physiol.* **168,** 1747–1761 (2015).
23. Correa-Galvis, V., Poschmann, G., Melzer, M., Stühler, K. & Jahns, P. PsbS interactions involved in the activation of energy dissipation in Arabidopsis. *Nature Plants* **2,** 15225 (2016).
24. Albanese, P. *et al.* Dynamic reorganization of photosystem II supercomplexes in response to variations in light intensities. *Biochim. Biophys. Acta*. **10,** 651–660 (2016).
25. Johnson, M.P., & Ruban, A.V. Arabidopsis plants lacking PsbS protein possess photoprotective energy dissipation. *Plant J.* **61,** 283–289 (2010).
26. Zia, A., Johnson, M.P., & Ruban, A.V. Acclimation- and mutation-induced enhancement of PsbS levels affects the kinetics of nonphotochemical quenching in *Arabidopsis thaliana*. *Planta* **233,** 1253–1264 (2011).

27. Belgio, E., Johnson, M.P., Jurić, S. & Ruban, A.V. Higher plant photosystem II light-harvesting antenna, not the reaction center, determines the excited-state lifetime - both the maximum and the nonphotochemically quenched. *Biophys. J.* **102,** 2761–2771 (2012).
28. Belgio, E., Ungerer, P. & Ruban, A.V. Light-harvesting superstructures of green plant chloroplasts lacking photosystems. *Plant, Cell and Environment* **38,** 2035–2047 (2015).
29. Ilioaia, C., Duffy, C.D.P. and Ruban, A.V. Changes in the energy transfer pathways within photosystem II antenna induced by the xanthophyll cycle activity. *J. Phys. Chem. B*, **117**, 5841–5847 (2013).
30. Johnson, M.P. *et al.* Photoprotective energy dissipation involves the reorganization of photosystem II light-harvesting complexes in the grana membranes of spinach chloroplasts. *Plant Cell* **23,** 1468–1479 (2011).
31. Ware, M.A., Giovagnetti, V., Belgio, E. & Ruban, A.V. PsbS protein modulates non-photochemical chlorophyll fluorescence quenching in membranes depleted from photosystems. *J. Photochem. Photobiol. B* **152**, 301–307 (2015).
32. Crouchman, S., Ruban, A. & Horton, P. PsbS enhances nonphotochemical fluorescence quenching in the absence of zeaxanthin. *FEBS Letters*. **580**, 2053–2058 (2006).
33. Kereïche, S., Kiss, A.Z., Kouril, R., Boekema, E. & Horton, P. The PsbS protein controls the macro-organisation of photosystem II complexes in the grana membranes of higher plant chloroplasts. *FEBS Letters* **584,** 754–764 (2010).
34. Goral, T. *et al.* Light-harvesting antenna composition controls the macrostructure and dynamics of thylakoid membranes in *Arabidopsis*. *Plant J.* **69,** 289–301 (2012).
35. Porra, R.J., Thompson, W.A. & Kriedemann, E.E. Determination of accurate extinction coefficients and simultaneous equations for assaying chlorophylls *a* and *b* extracted with four different solvents: verification of the concentration of chlorophyll standards by atomic absorption spectroscopy. *Biochim. Biophys. Acta* **975,** 384–394 (1989).
36. Ruban, A.V. *et al.* Plasticity in the composition of the light harvesting antenna of higher plants preserves structural integrity and biological function. *J. Biol. Chem.* **281,** 14981–14990 (2006).
37. Laemmli, U.K. Cleavage of structural proteins during the assembly of the head of bacteriophage T4. *Nature* **227**, 680–685 (1970).
38. Kouřil, R., Dekker, J.P., Boekema, E.J. Supramolecular Structure of photosystem II in green plants. *Biochim. Biophys. Acta* **1817,** 2–12 (2012).

ACKNOWLEDGEMENTS. A.V.R acknowledges funding from the Biotechnology and Biological Sciences Research Council of UK and The Leverhulme trust. The authors acknowledge Yonglan Tian for the help with plant growth, as well as Matt Johnson and Christopher Duffy for critical reading of the manuscript.

AUTHOR CONTRIBUTIONS. J.S. and A.V.R. designed experiments. J.S. performed biochemistry, PAM fluorescence measurements, preparation for TEM and particle analysis. V.G. performed PAM fluorescence measurements. P.U. assisted with experiments. G.M. operated TEM and assisted with sample preparation. All authors discussed the results and commented upon the manuscript. J.S., V.G. and A.V.R. wrote the manuscript.

FIGURE LEGENDS

Figure 1 | Affinity pull-down assay on violaxanthin-containing spinach membranes. (a) Comparison and identification of interacting protein partners without (-) and with (+) cross-linker (DSP, 0.5 mM) by separation of equal elution volumes on SDS-PAGE followed by western blotting with Lhcb1-6 antibodies. Th, thylakoid membranes. (b) Quantification of LHCII subunits associated with PsbS protein without (-DSP) and with cross-linker (+DSP). Data have been normalized to the total amount of isolated PsbS. Each lhcb polypeptide has been quantified using all bands detected in the lane. Data are averages of three biological replicates ± SD. Asterisks represent statistical significant changes ($P<0.05$) between dark/NPQ (*) and NPQ/recovery states (**). (c) Representative PAM chlorophyll fluorescence trace measured on chloroplasts prior to isolation procedure. Black arrows mark sample state. (d) Western blotting following PsbS pull-down assay on D1 protein of photosystem II reaction center in chloroplasts dark-adapted, and in NPQ and recovery state (+/- DSP).

Figure 2 | Affinity pull-down assay on zeaxanthin-containing spinach membranes. (a) Comparison and identification of interacting protein partners without (-) and with (+) cross-linker (DSP, 0.5 mM) by separation of equal elution volumes on SDS-PAGE followed by western blotting with Lhcb1-6 antibodies. Th, thylakoid membranes. (b) Quantification of LHCII subunits associated with PsbS protein without (-DSP) and with cross-linker (+DSP). Data have been normalized to the total amount of isolated PsbS. Each lhcb polypeptide has been quantified using all bands detected in the lane. Data are averages of three biological replicates ± SD. Asterisks

represent statistical significant changes (P<0.05) between dark/NPQ (*) and NPQ/recovery states (**). (c) Representative PAM chlorophyll fluorescence trace measured on chloroplasts prior to isolation procedure. Black arrows mark sample state.

Figure 3 | FPLC gel-filtration separation of *A. thaliana L17* membranes in dark and NPQ state. (a) Trace recorded during FPLC gel-filtration separation (670 nm-red, at 435 nm-magenta and 280 nm-blue). Marked fractions (B11-B1) were collected for further analysis. (b) Separation on SDS-PAGE of FPLC fractions. Proteins were stained with Instant Blue. (c) Immunoblot identification of Lhcb1, PsbS and CP29 proteins.

Figure 4 | Localization of PsbS in dark-adapted and light-treated spinach chloroplasts based upon the electron microscopy of immuno-gold labelled negatively stained thin-sections of the fixed material. (a) Thin section images and enlarged images of the original micrographs marked with 50 nm radius areas used to calculate the number of neighbouring particles. (b) Quantification of PsbS particles found within a 50 nm radius area in the dark and NPQ state. (c) Changes in the density of PsbS gold particles upon illumination. More than 30000 particles from three biological replicates were picked and used to calculate averages ± SD. Asterisks (*) indicate statistical significant changes (P<0.05).

Figure 5 | Model of PsbS interactions within PSII-LHCII complex. The model depicts PsbS localizations in relation to PSII core complex (RCII) and LHCII antenna in violaxanthin-containing photosynthetic membranes (dark-adapted and in NPQ state), and in zeaxanthin-containing photosynthetic membranes (dark-adapted and in NPQ state). Red subunits represent PSII dimers, grey subunits indicate the position of minor antenna (CP29, CP26 and CP24), while white and blue subunits that of LHCII trimers according to their binding to RCII: strongly (S), moderately (M) and loosely (L) bound LHCII trimers[38]. Big and small black subunits are PsbS dimers and monomers, respectively. Numbers in red indicate the monomeric LHC complexes that interact with PsbS.

Sacharz et al., Figure 1.

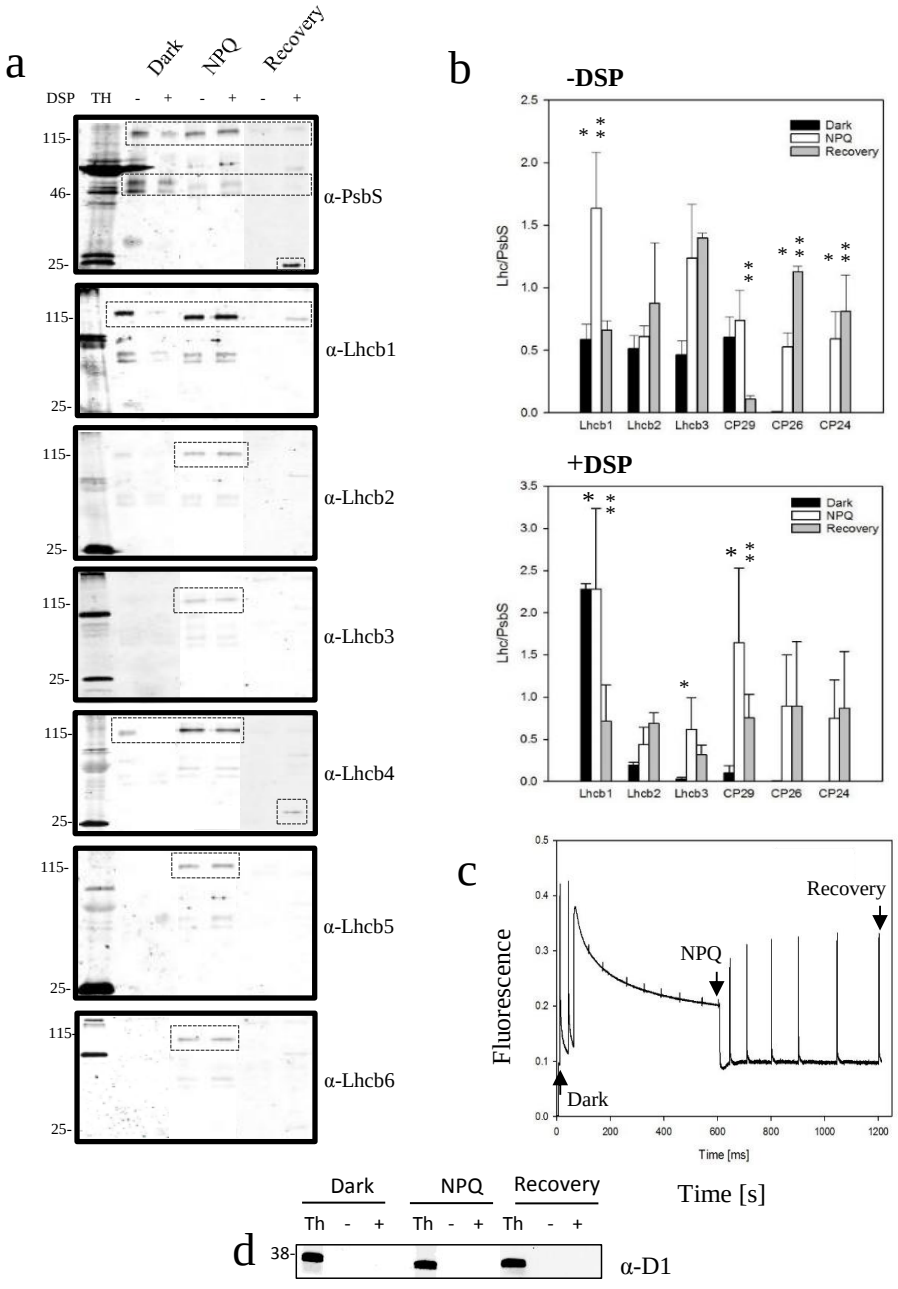

Figure 1 | Affinity pull-down assay on violaxanthin-containing spinach membranes. (a) Comparison and identification of interacting protein partners without (-) and with (+) cross-linker (DSP, 0.5 mM) by separation of equal elution volumes on SDS-PAGE followed by western blotting with Lhcb1-6 antibodies. Th, thylakoid membranes. (b) Quantification of LHCII subunits associated with PsbS protein without (-DSP) and with cross-linker (+DSP). Data have been normalized to the total amount of isolated PsbS. Each lhcb polypeptide has been quantified using all bands detected in the lane. Data are averages of three biological replicates ± SD. Asterisks represent statistical significant changes ($P<0.05$) between dark/NPQ (*) and NPQ/recovery states (**). (c) Representative PAM chlorophyll fluorescence trace measured on chloroplasts prior to isolation procedure. Black arrows mark sample state.

554

Sacharz et al., Figure 2.

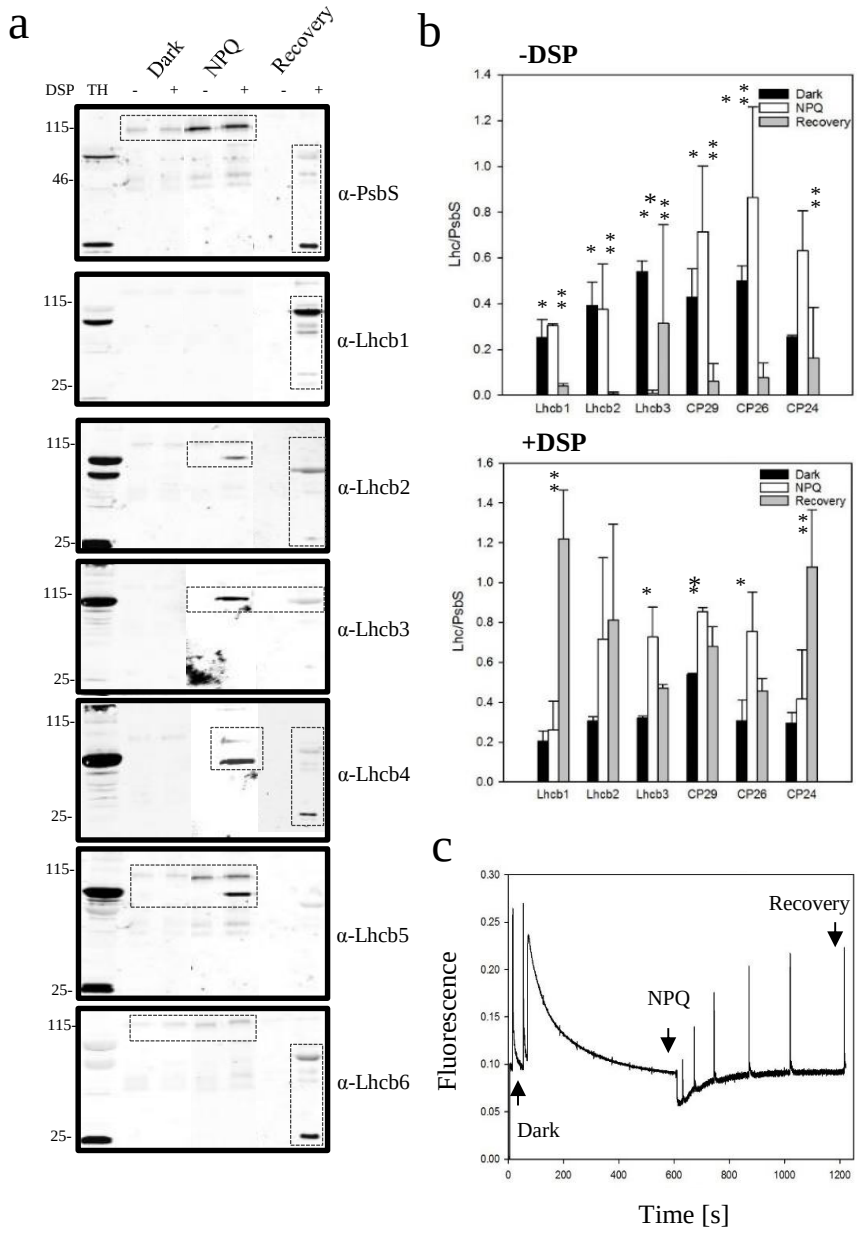

Figure 2 | Affinity pull-down assay on zeaxanthin-containing spinach membranes. (a) Comparison and identification of interacting protein partners without (-) and with (+) cross-linker (DSP, 0.5 mM) by separation of equal elution volumes on SDS-PAGE followed by western blotting with Lhcb1-6 antibodies. Th, thylakoid membranes. (b) Quantification of LHCII subunits associated with PsbS protein without (-DSP) and with cross-linker (+DSP). Data have been normalized to the total amount of isolated PsbS. Data are averages of three biological replicates ± SD. Asterisks represent statistical significant changes ($P<0.05$) between dark/NPQ (*) and NPQ/recovery states (**). (c) Representative PAM chlorophyll fluorescence trace measured on chloroplasts prior to isolation procedure. Black arrows mark sample state.

555

Sacharz et al., Figure 3.

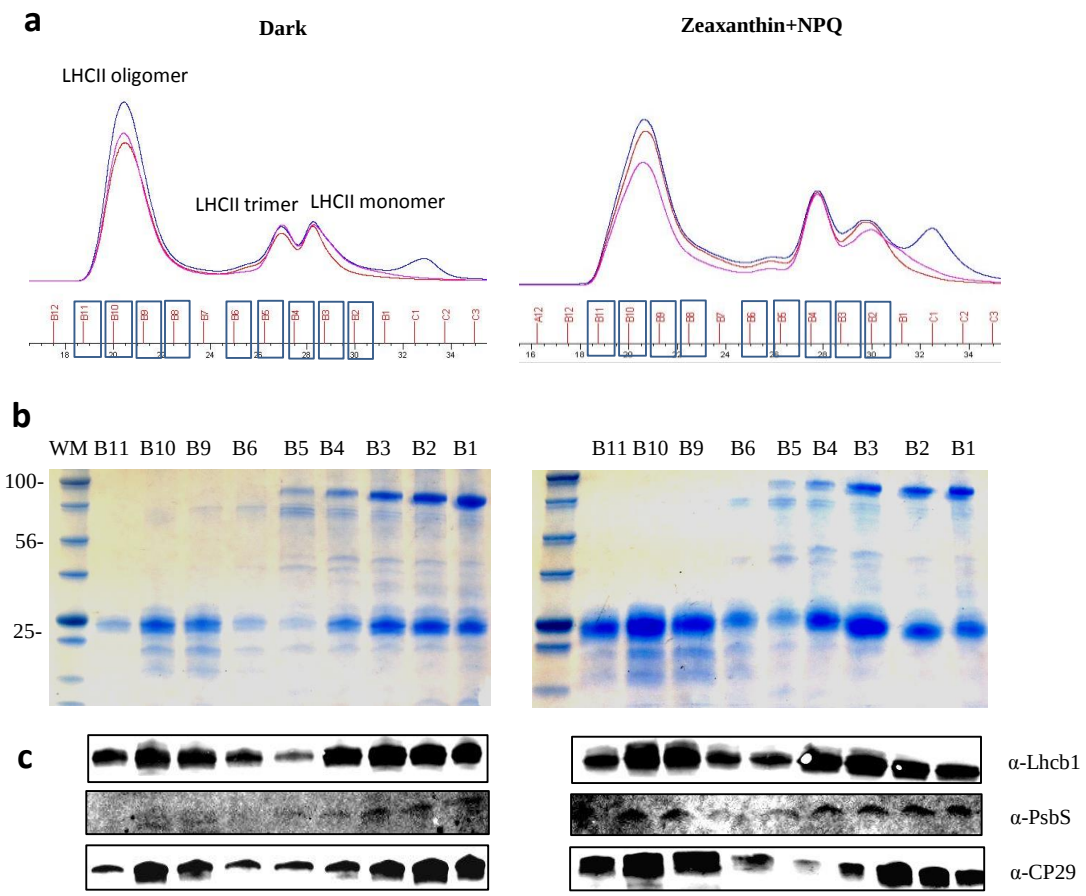

Figure 3 | FPLC gel-filtration separation of *A. thaliana L17* membranes in dark and NPQ state. (a) Trace recorded during FPLC gel-filtration separation (670 nm-red, at 435 nm-magenta and 280 nm-blue). Marked fractions (B11-B1) were collected for further analysis. (b) Separation on SDS-PAGE of FPLC fractions. Proteins were stained with Instant Blue. (c) Immunoblot identification of Lhcb1, PsbS and CP29 proteins.

559

Sacharz et al., Figure 4.

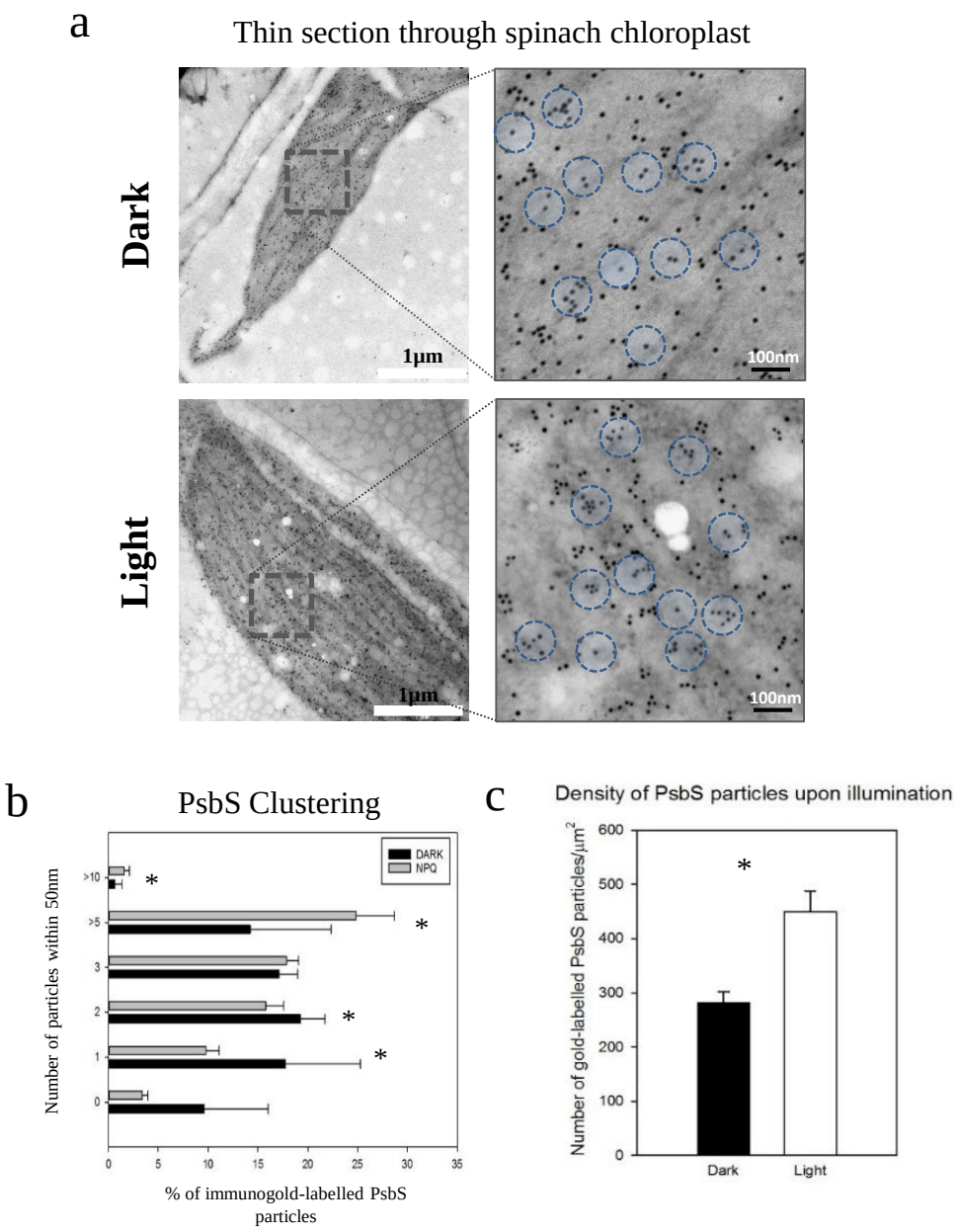

Figure 4 | Localization of PsbS in dark-adapted and light-treated spinach chloroplasts based upon the electron microscopy of immuno-gold labelled negatively stained thin-sections of the fixed material. (a) Thin section images and enlarged images of the original micrographs marked with 50 nm radius areas used to calculate the number of neighbouring particles. (b) Quantification of PsbS particles found within a 50 nm radius area in the dark and NPQ state. (c) Changes in the density of PsbS gold particles upon illumination. More than 30000 particles from three biological replicates were picked and used to calculate averages ± SD. Asterisks (*) indicate statistical significant changes ($P<0.05$).

Sacharz et al., Figure 5.

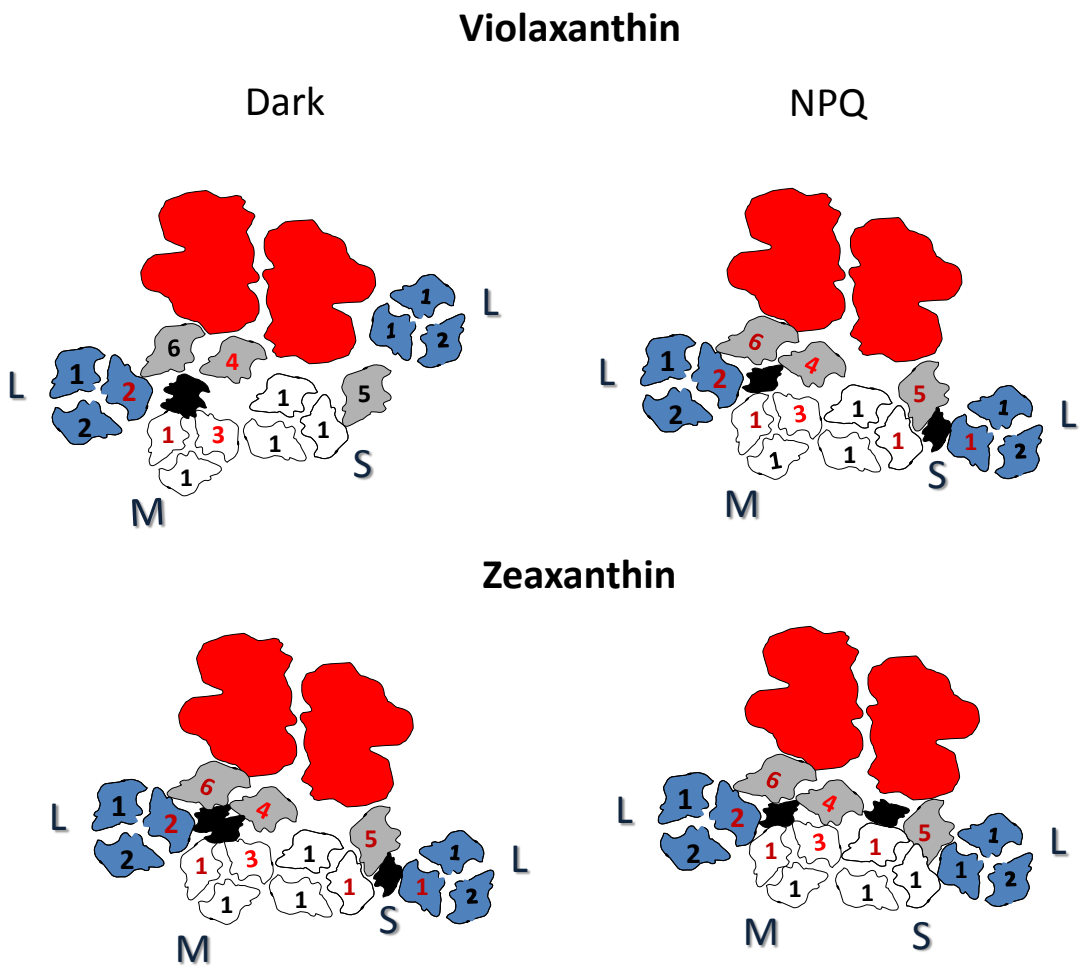

Figure 5 | The model of PsbS interactions within PSII-LHCII complex. The model depicts PsbS localizations in relation to PSII core complex (RCII) and LHCII antenna in violaxanthin-containing photosynthetic membranes (dark-adapted and in NPQ state), and in zeaxanthin-containing photosynthetic membranes (dark-adapted and in NPQ state). Red subunits represent PSII dimers, grey subunits indicate the position of minor antenna (CP29, CP26 and CP24), while white and blue subunits that of LHCII trimers according to their binding to RCII: strongly (S), moderately (M) and loosely (L) bound LHCII trimers38. Big and small black subunits are PsbS dimers and monomers, respectively. Numbers in red indicate the monomeric LHC complexes that interact with PsbS.

560